



City Research Online

City, University of London Institutional Repository

Citation: Bigdeli, A., Vosoughi, S., Tsavdaridis, K., Eslamnia, H. & Farajian, M. (2025). Seismic Risk Assessment of Steel Volumetric Modular Buildings under the Mainshock-Aftershock Ground Motions. Structures, 76, 108960. doi: 10.1016/j.istruc.2025.108960

This is the accepted version of the paper.

This version of the publication may differ from the final published version.

Permanent repository link: <https://openaccess.city.ac.uk/id/eprint/35037/>

Link to published version: <https://doi.org/10.1016/j.istruc.2025.108960>

Copyright: City Research Online aims to make research outputs of City, University of London available to a wider audience. Copyright and Moral Rights remain with the author(s) and/or copyright holders. URLs from City Research Online may be freely distributed and linked to.

Reuse: Copies of full items can be used for personal research or study, educational, or not-for-profit purposes without prior permission or charge. Provided that the authors, title and full bibliographic details are credited, a hyperlink and/or URL is given for the original metadata page and the content is not changed in any way.

Seismic Risk Assessment of Steel Volumetric Modular Buildings under the Mainshock-Aftershock Ground Motions

Ali Bigdeli^a, Sadegh Vosoughi^b, Konstantinos Daniel Tsavdaridis^{c*}, Hadi Eslamnia^d,
Mostafa Farajian^e

^a Department of Civil and Environmental Engineering, Tarbiat Modares University, Tehran, Iran

^b Department of Civil and Environmental Engineering, South Tehran branch, Islamic Azad University, Tehran, Iran

^c Department of Engineering, School of Science & Technology, City St George's, University of London,
Northampton Square, EC1V 0HB, London, UK

^d Department of Civil and Environmental Engineering, Amirkabir University of Technology, Tehran, Iran

^e Department of Civil and Environmental Engineering, Semnan University, Semnan, Iran

*Corresponding author: Konstantinos.tsavdaridis@city.ac.uk

Abstract

A mainshock-aftershock sequence can pose a substantial threat to buildings in seismically active areas, especially those that have already been damaged or weakened by an earlier earthquake. The damage progression and cumulative damage, as well as degradation of strength and stiffness, may result in a structure collapsing under a strong aftershock. This study addresses a critical research gap by evaluating the seismic response of corner-supported steel modular building systems (MBSs) subjected to sequential mainshock-aftershock (MS-AS) scenarios. Unlike conventional steel structures, MBSs exhibit distinct dynamic characteristics due to their modular connections. The current study identifies these limitations and presents the first fragility analysis that is specific for MBSs. Therefore, this paper aims to analyse the seismic risk assessment of corner-supported steel volumetric braced MBSs during sequential earthquake events, with emphasis on MS-AS sequences. The study explores how aftershocks affect the performance of modular buildings, particularly when initial mainshocks have already caused damage. Based on the equations proposed by FEMA P58, it considers four damage states with respect to maximum inter-story drift. MBSs are modeled using OpenSees software using the modified Ibarra-Median-Krawinkler model. The structural responses of MBS models of varying heights (4, 8, and 12 storeys) are captured by a suitable number of nonlinear dynamic analyses using Incremental Dynamic Analysis (IDA). Under MS-AS sequences, fragility curves can be obtained to quantify the likelihood of surpassing different DSs for MBSs. The Collapse Margin Ratio (CMR) can be used to assess the resilience of MBSs at different damage states by examining structural collapse probabilities. Results show that aftershocks significantly increase the likelihood of collapse of modular buildings, in particular those severely damaged by major earthquakes. Fragility curves confirm this, indicating an increased collapse probability across all building heights for higher damage states. When buildings are subjected to aftershock sequences, their CMR values are decreased on average by 9.9%, 13.17%, and 6.5% for 4-, 8-, and 12-story MBSs, respectively. The findings emphasize the importance of incorporating aftershock considerations into MBS design standards to enhance earthquake resilience and safety.

Keywords: Modular Steel Buildings; Collapse risk; Mainshock–aftershock sequence; FEMA P-58; Fragility curves; Residual drift; Collapse Margin Ratio

1. Introduction

In seismically active areas, mainshock-aftershock sequences are frequently observed, where a large earthquake (mainshock, MS) is followed by multiple smaller earthquakes (aftershocks, AS) within a short period of time. Aftershocks can cause considerable damage to structures, especially if these structures have already been weakened or damaged by the main earthquake. Multiple aftershocks can contribute to further structural and building failure by destabilizing buildings, bridges, and other infrastructure [1-5]. Aftershocks can therefore result in considerable structural damage and fatalities [3]. In spite of this, the current seismic design philosophy is primarily concerned with controlling the dynamic response of structures in the event of a single earthquake without taking into account the detrimental effects of subsequent earthquakes [4]. Consequently, it is essential to conduct a comprehensive investigation into the seismic safety assessment of modular structures that are subjected to mainshock-aftershock sequences to implement appropriate seismic protection measures.

Modular Buildings Systems (MBS) is a modern method of construction (aka MMC) whereby the various components of steel volumetric modular units, that include walls, studs, floors, and ceilings, are manufactured off-site efficiently and precisely, and assembled on the construction site to create a single integrated building [5–8]. It offers high quality, accurate completion timelines, and waste material reduction. Due to the lack of clear regulations or guidelines for design or compliance criteria, this type of construction is mainly designed based on conventional design guidelines and light modifications where necessary [9]. The seismic risk assessment of MBSs, particularly considering the complex loading scenarios posed by mainshock-aftershock sequences, remains a significant area of research, especially given that the dynamic properties of such buildings may not be calculated using the relevant common equations developed for conventional buildings [10].

A volumetric module (container like structure) can be classified based on its load transfer mechanism either as a load-bearing wall or a corner-supported frame. In the former module, The four side walls transfer the gravity load to the base, whereas in the latter one, the corner posts and edge beams are responsible for transferring the load [11]. In high-rise buildings, corner-supported modules are commonly used due to their capacity to carry heavy loads [12]. An MBS is composed of multiple modular units that are interconnected through inter-module connections. Inter-module

connections include both horizontal and vertical connections. Vertical connections transfer load between upper and lower modules, whereas horizontal connections are defined as connections between adjacent modules [13,14].

Extensive research conducted studying the effects of mainshock-aftershock (MS-AS) sequences on various types of structures including hydraulic structures [15–17], transmission towers [18,19], storage tanks [20], bridges [21], underground structures [22,23], and masonry structures [24,25]. With regard to the effects of MS-AS sequences on buildings, Koohfallah et al. investigated various scenarios of the impact of MS-AS to identify the most effective option for retrofitting a school building [26]. According to their analysis of the impact of MS-AS on seismic resilience index of schools, an increase in mainshock damage results in an increase in repair costs and repair times, which results in a reduction in the resilience index. Buildings equipped with friction dampers have been evaluated for seismic performance in MS–AS sequences, according to Rayegani et al. [27]. Retrofitted structures with these dampers showed little impact on the displacements or residual displacements caused by aftershocks. A fragility framework was developed by Saed and Balomenos for three corroded steel frame structures using reduced beam section (RBS) connections influenced by MS–AS sequences[28]. The researchers concluded that maximum inter-story drift ratios based on damage states provide more reliable criteria for determining the seismic fragility curves of SMRF structures than residual inter-story drift ratios. Another study was conducted to assess the seismic fragility and loss estimates of self-centering braced frames (SCBs) [29]. According to their findings, for buildings with single- and dual-core frames, the probability of collapse increases from 18% to 28% and from 10% to 16%, respectively, when aftershocks are also considered. Moreover, they discovered that MS-AS sequences had a minimal impact on both structures' maximum absolute floor acceleration. Jalali et al. evaluated the impact of MS-AS sequences on the collapse of steel plate shear walls (SPSWs) [30]. To evaluate the plastic behavior of 9-story, 14-story, and 20-story SPSWs in large inelasticity regions, static-pushover analyses have been conducted, followed by incremental dynamic analyses to assess the collapse capacity under aftershocks preceding mainshocks. The web plates provided less participation for absorbing the aftershock energy in stories where plates absorbed significant energy during the mainshock. An investigation based on the collapse mechanisms of Special Steel Moment Frames (SSMFs) under aftershock events preceded by different levels of mainshocks was carried out by Torfehnejad and Sensoy [31]. Based on their findings, the mainshock damage

and the resulting behavioral degradation of a member reduced the ability for the member to absorb energy at the point of collapse caused by the aftershock. Shafaei and Naderpour investigated the collapse capacity of reinforced concrete buildings when MS-AS impacts are considered [32]. An evaluation of the collapse capacity of ordinary RC frames with four, eight, and twelve stories was performed under aftershock earthquakes. The maximum story drift distribution along the buildings' heights at collapse states caused by aftershocks, the failure mechanism of the buildings was not largely influenced by the damage caused by the main shock. The probabilistic seismic demand model and structural demand hazard curve were examined for steel buildings with and without bracing systems incorporating shape memory alloys during MS-AS sequences by Shi et al. [33]. The results demonstrated that a steel frame building equipped with SMA braces will function more effectively following a major event. Hassan et al. investigated the response of semi-rigid steel frames to earthquake ground motions sequences [34]. The aim of this study was to design and evaluate three semi-rigid frames with various connection capacities of the beam's plastic moment, and to evaluate their seismic performance under the action of MS-AS sequences. Based on the results, aftershock inclusion increases the likelihood that the frames will reach a specific damage state or exceed it, mainly because of the period elongation resulting from the induced permanent damage.

Investigating the seismic behavior of steel volumetric MBSs, several studies have been conducted. Emamikoupaie et al. investigated the effect of near-field earthquakes on modular steel buildings (MSB) [35]. Fathieh and Mercan studied the seismic performance of MSBs [36]. Batukan et al. studied the Seismic performance of MSBs equipped with resilient slip friction joints [37]. Annan and Youssef examined the evaluation of seismic vulnerability in MSBs [38]. Chua et al. studied the lateral behavior of high-rise steel volumetric MBSs [39]. Peng et al. investigated the lateral load resistance of multi-story modular structures [40]. Lacey et al. studied the lateral behavior of MSBs using simplified models of novel inter-module connections [41]. Although these studies have opened new insights into the seismic performance of MBSs, all the investigations mentioned above take ground motion input only from mainshocks. There has been evidence, however, that most earthquakes with higher magnitudes are often accompanied by a series of aftershocks within a short period of time [4]. The literature lacks comprehensive studies specifically investigating the seismic performance of MBSs under mainshock-aftershock

sequences. Existing research often focuses on single earthquake events, neglecting the cumulative damage effects of multiple seismic events.

The endeavor to evaluate the effect of earthquake sequences on this type of building can make a meaningful contribution to complement previous studies of the seismic performance of MBSs.

Based on the abovementioned discussions, the main objective of this study is to investigate the seismic risk assessment of modular building systems considering the effect of sequential earthquake ground motions. For this, three steel corner supported braced frame MBSs with 4-, 8-, and 12-story are subjected to the MS-AS earthquakes. Incremental dynamic analysis (IDA) is performed using a suite of mainshocks and aftershocks records to capture the nonlinear seismic response of MBSs including maximum inter-story drift, residual drift ratio, and roof drift. Then, a seismic fragility assessment curve is developed for the steel-braced frame MBSs under the MS-AS sequence. Finally, the collapse capacity of the MBSs is quantified by determining the value of the collapse margin ratio. This study can provide a reference for the seismic risk assessment and safety evaluation of MBSs.

2. Methodology

2.1 Incremental Dynamic Analysis (IDA)

IDA is commonly used to calculate EDPs for buildings under MS and MA-AS sequences, as well as to develop the capacity curves of the buildings [42]. A collection of chosen ground motion records is employed to perform multiple nonlinear time-history (NLTH) analyses on the selected structures. The ground motion records are scaled incrementally to a specific seismic intensity and a dynamic NLTH analysis is carried out to capture the structure's entire response from elastic behavior to collapse [43]. Based on the assumption that the steel MBSs are located far away from active faults, far-fault earthquake records are used to evaluate them in this study. To determine the collapse point, two criteria are considered. According to FEMA 350 [44], an initial collapse criterion is the intensity level where the local slope of the IDA curve drops below 20% of its initial slope. A second criterion is determined by the transient inter-story drift ratio and residual drift ratio of the collapse point, in accordance with the damage states defined in the next sections.

IDA is performed using two methods. A fixed-step method involves incrementally scaling records with constant values (normally with 0.1g intervals). While the fixed-step method is simple and straightforward, however, it may not provide accurate results at collapse points. Therefore, another method that is more efficient and accurate, and the IDA curve is drawn with sufficient accuracy and speed, is the hunt and fill algorithm [43]. The Hunt and Fill algorithm was preferred over a fixed-step method due to its higher computational efficiency and ability to adaptively capture structural responses near collapse, reducing unnecessary analyses at low-intensity levels and improving numerical stability. In this approach, to minimize the number of analyses, each record is scaled to cover all structural responses using this algorithm. As the structure reaches its ultimate state (collapse point), additional analyses are conducted at lower IM levels to improve the IDA curve's accuracy.

IDA process with hunt and fill algorithms consists of three steps. The first step, known as the Hunt stage, consists of reaching the ultimate damage limit state as quickly as possible. To accomplish this, scaling records are increased progressively as shown in Eq. (1). During this stage, two points are determined, including the collapse point and the non-collapse point. It is worth noting, however, that the value of the collapse point is not reliable at this stage.

$$IM_{new} = IM_{old} + n.\Delta IM \quad (1)$$

The Bracket stage determines the accurate collapse point after determining the interval between collapse (C) and non-collapse (NC) points. Based on Eq. (2), this interval becomes small and an accurate collapse point can be determined. It should be mentioned that in this study, the tolerance value of 0.05 is considered in this study to indicate the end of this stage.

$$IM_{new} = IM_{NC} + (IM_C - IM_{NC})/3 \quad (2)$$

To ensure that the accuracy is improved at the lower levels of considered IM, during the final stage of the process, known as the Fill stage, further analyses are conducted at intermediate IM levels.

2.2 Intensity Measures (IMs) and Engineering Demand Parameters (EDPs)

An engineering demand parameter (EDP) represents the seismic response characteristics of a structure. Engineering demand parameters are primarily determined by two parameters: the peak

Inter-story Drift Ratio (IDR), and peak residual inter-story drift (RIDR) which is another important metric to identify potential damage levels and assess resilience.

According to previous studies, it is crucial to choose appropriate intensity measures, which will be scalable and represent the main characteristics of an earthquake, including its amplitude, duration, frequency content, etc. In addition, it should have the greatest correlation with EDPs. To include the structure's period time and damping parameters in the scaling, spectral acceleration at the first mode was selected as IM. The previous study of optimal IMs for steel modular buildings also found that $S_a(T_1, 5\%)$ is the optimal IM for steel modular buildings [9].

2.3 Fragility Assessment

It is crucial to calculate fragility curves after a mainshock and an aftershock sequence in order to determine structural vulnerability as together they take into account cumulative damage and the deterioration of structural capacity. These curves provide probabilistic estimates of damage states post-mainshock, which aid in assessing failure risks and guiding resilient design strategies that will ensure safety in the event of repeated earthquakes.

Fragility curve is developed based on statistical analysis of structural response data obtained from nonlinear dynamic analyses of the structure under different earthquake intensities. IDAs are conducted with a suite of earthquake ground motion recordings for the generation of fragility curves to represent different seismic intensity levels, and appropriate damage states are determined based on EDP, which is a direct reflection of structural damage. Then, a probabilistic calculation of the likelihood that the structural response will exceed the predefined threshold is performed for each limit state under different levels of Intensity Measures (IM).

A fragility curve is usually represented by a lognormal cumulative distribution function (CDF), which has two parameters: median IM and log standard deviation. Fragility can be expressed in the following way:

$$P[EDP \geq edp | IM] = 1 - \Phi \left(\frac{\ln(edp) - \ln(\eta_{EDP|IM})}{\beta_{EDP|IM}} \right) \quad (2)$$

where $\Phi(\cdot)$ is the ‘standardized’ Gaussian cumulative distribution function, $\eta_{EDP|IM}$ is the median value of the intensity measure (IM) at which the specified EDP threshold (edp) is exceeded, and

$\beta_{EDP|IM}$ is the logarithmic standard deviation or dispersion associated with the variability in IM corresponding to the exceedance of the EDP threshold. In addition, the relationship between EDP and IM is stated in the power form according to the Eq. (3):

$$\eta_{EDP|IM} = a (IM)^b \quad (3)$$

Equation for linear regression has two constant parameters, a and b. Eq. (3) can also be represented in lognormal space, as depicted in Eq. (4):

$$\ln(\eta_{EDP|IM}) = b \cdot \ln(IM) + \ln(a) \quad (4)$$

In this equation, $\ln(a)$ represents the vertical intercept, while b represents the slope constant. Based on nonlinear time history analyses of selected MBS models, regression data is generated for N analysis. According to Eq. (5), the N demand quantities are plotted against the IM so that the regression parameters and dispersion term can be estimated.

$$\beta_{EDP|IM} \cong \sqrt{\frac{\sum_{i=1}^n (\ln(edp_i) - \ln(\eta_{EDP|IM}))^2}{n-2}} \quad (5)$$

In this instance, n represents the number of analyses, and edp_i represents the i^{th} realization of EDP from the nonlinear time history analysis.

2.4 Damage Limit States

For assessing the MBS's performance after an MS-AS sequence, damage limit states are essential. A variety of performance indicators have been used to quantify the risk of aftershock collapse caused by the mainshock events. To describe these states, the IDR is often used, since MBS behavior is driven by deformation, and IDR is one of the best methods of representing deformation [45]. Moreover, previous research highlighted the significance of residual drifts in seismic design, recognizing them as a crucial metric for assessing seismic performance [46,47]. Residual drifts have been examined further in order to evaluate multi-story frame buildings and their performance [33,48]. For predicting the collapse capacity of steel frame structures subjected to aftershocks, Ruiz-Garcia [49] proposed using RIDR as a damage indicator.

To define the initial mainshock damage states, a maximum of the IDR was used. As a first step, peak RIDR values were chosen based on four performance levels (0.2%, 0.5%, 1%, and 2%) recommended in FEMA P-58 [50]. IDR cannot be measured directly during an earthquake, but RIDR can be measured following an earthquake. This relationship between IDR and RIDR is therefore provided in seismic guidelines to estimate the IDR that occurred during a particular earthquake with a greater degree of accuracy. The limit states in this study are defined according to FEMA P-58 by defining four post-mainshock damage states based on peak IDR, where RIDR and IDR are related as shown in the following equations. To compare the peak IDR ratios for each MS limit state to the limit states defined on the basis of RIDRs, the ratios were selected in such a way that they are comparable.

$$\Delta_r = 0 \text{ for } \Delta \leq \Delta_y \quad (6)$$

$$\Delta_r = 0.3 \times (\Delta - \Delta_y) \text{ for } \Delta_y \leq \Delta \leq 4\Delta_y \quad (7)$$

$$\Delta_r = \Delta - 3 \times \Delta_y \text{ for } \Delta \geq 4\Delta_y \quad (8)$$

where, Δ_y is the yield story drift, which is obtained from pushover analysis, Δ_r and Δ are RIDR and IDR, respectively. From a pushover analysis, the story drift at the yield point of each evaluated MBS is calculated as 0.6% for four stories, 1% for eight stories, and 1.5% for twelve stories for each limit state. Each limit state's IDR value is then calculated based on Eq. (6)- Eq. (8). Table 1 summarizes the damage states considered in this study under the mainshock records. It should be mentioned that in the mainshock records, the MBSs reach the three first damage states (DS1-DS3), and the damage state corresponding to the collapse point (DS4) is taken into account in the mainshock-aftershock analysis.

Table 1 considered IDR for each Damage state based on RIDR limit states

MBS story	DS1 (%)	DS2 (%)	DS3 (%)	DS4 (%)
4-story	1.5	2.5	3.0	4.0
8-story	2.0	3.0	4.0	5.0
12-story	2.0	3.0	5.0	6.0

3. Ground Motion Records

In seismic studies, there are three main methods to select ground motions: Repeated [74,75], randomized [76,77], and as-recorded sequence [29]. The repeated approach applies the same

ground motion which will produce demand at a consistent level but without natural variability. Alternatively, randomized methods provide a wide range of seismic scenarios and account for some structural variability by randomly selecting ground motions. As-recorded ground motion sequences yield realistic sequence effects but require extensive data collection to produce realistic sequence effects. The randomized approach was adopted in this study to achieve a wide representation of possible seismic events and capture variability in the response of modular buildings.

For this purpose, a total of 10 ground motion records from FEMA P-695 study [45] was utilized as MS and AS earthquakes to examine the impact of mainshock-aftershock sequences on modular buildings. In each analysis, one record is the mainshock, while the remaining nine records are considered to be aftershocks. The first step in the process is to conduct IDA analysis on the mainshock records to identify the intensities that lead to the specified damage states. Then by using NLTH, the structure was first subjected to a mainshock scaled to induce a specific damage state (DS1–DS3). Following, the IDA is carried out on the aftershock records to assess cumulative damage. The process is repeated for each record, with each one serving as the mainshock once, creating a total of 90 mainshock-aftershock combinations. This method allows for the comprehensive examination of structural responses under a variety of sequence scenarios, which effectively captures aftershock effects and provides robust insight into the cumulative damage and collapse risk for structures subjected to sequential seismic events. Figure 1 shows the schematic view of the process.

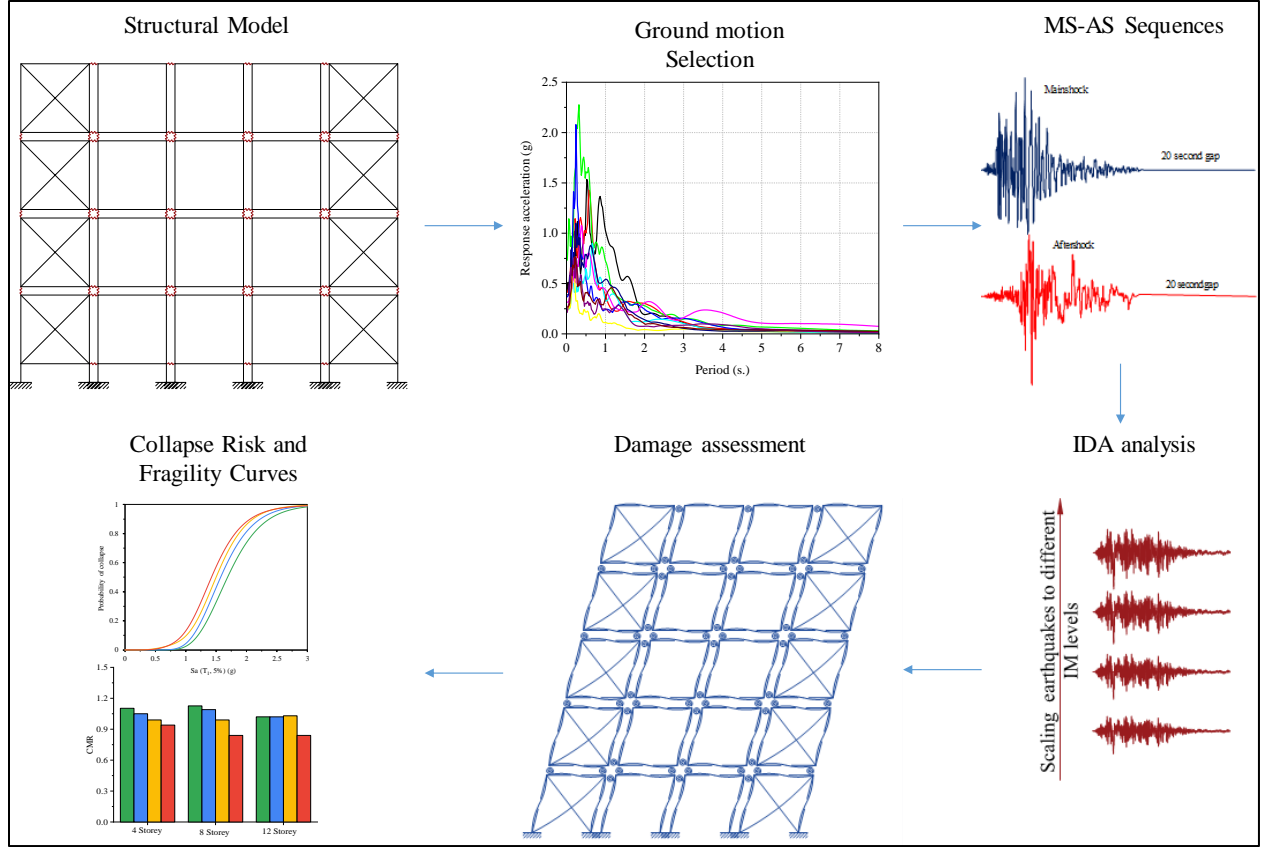


Figure 1 Illustration of the process involved in developing MS-AS fragility curves for MBSs.

Comprehensive details of the considered earthquake ground motions are presented in Table 2. In selecting ground motions, distinct earthquake characteristics, including their amplitude, frequency content, and duration are considered. Site-source distances range between 7.9 km and 22.8 km for the selected records, with magnitudes varying from M6.5 to M7.5, ground acceleration peak values ranging from 0.21 g to 0.73 g, and ground velocity peak values ranging from 19 cm/s to 59 cm/s. The selected ground motions were not limited to a specific site class but were chosen randomly to ensure a broad seismological diversity, including variations in magnitude, source-to-site distance, duration, and frequency content. Figure 2 illustrates the elastic spectra of considered earthquake ground motions considering a viscous damping ratio of 5%.

Table 2 Details of selected Ground motions

Record No.	Event	Year	Station	M_w	PGA(g)	PGV(cm/s)
1	Northridge	1994	Beverly Hills	6.7	0.41	58

2	Northridge	1994	Canyon Country	6.7	0.48	45
3	Duzce, Turkey	1999	Bolu	7.1	0.73	56
4	Imperial Valley	1979	El Centro	6.5	0.36	34
5	Kobe	1995	Shin-Osaka	6.9	0.24	38
6	Kocaeli	1999	Duzce	7.5	0.31	59
7	Kocaeli	1999	Arcelik	7.5	0.22	17
8	Cape Mendocino	1992	Rio Dell Overpass	7.0	0.55	44
9	San Fernando	1971	LA-Hollywood Stor	6.6	0.21	19
10	Hector Mine	1999	Hector	7.1	0.34	42

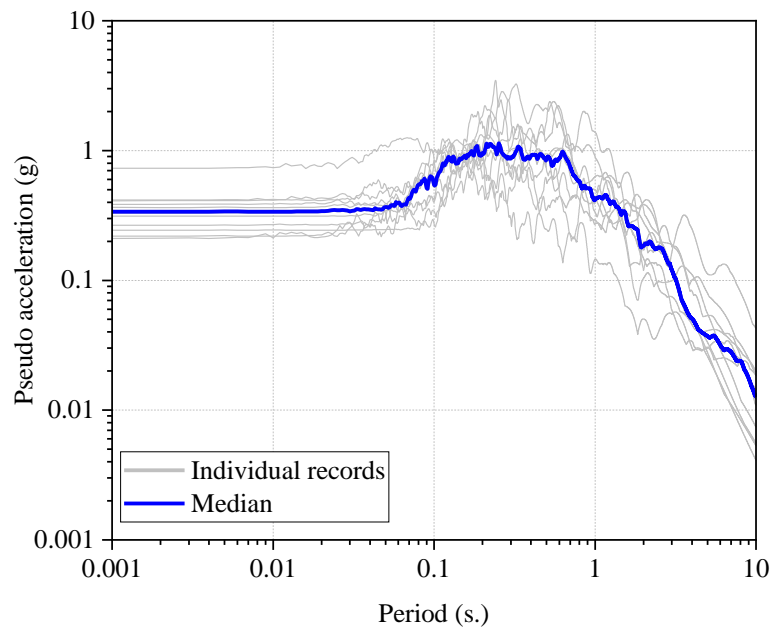


Figure 2 Acceleration response spectra of the selected ground motion records

As can be seen in Figure 3, there is a 20-second gap between two consecutive seismic events as well as at the end of the aftershock record. In this gap, there is no acceleration ordinate, and it is enough for the structure to stop moving after it has experienced the previous seismic event.

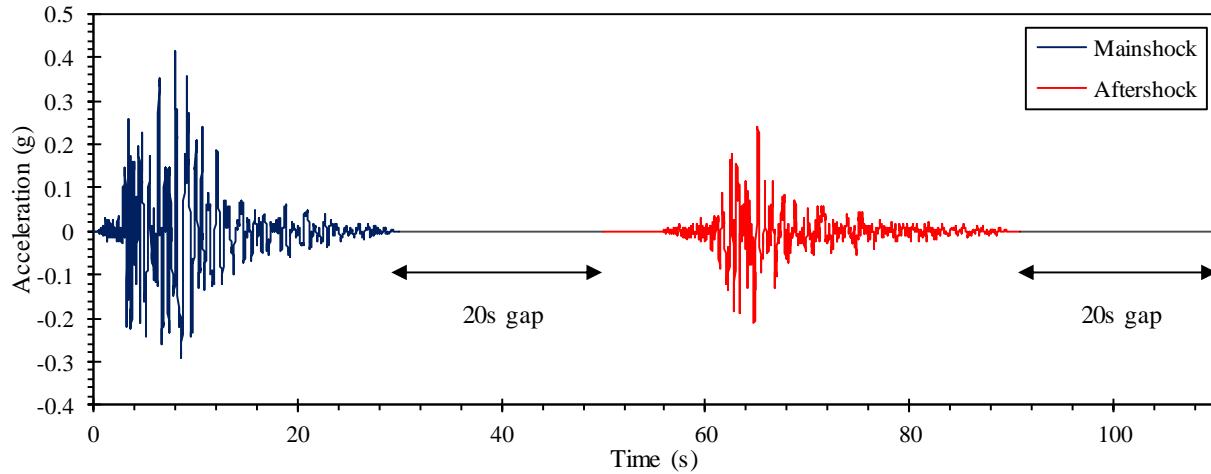


Figure 3 Input acceleration time history of MS-AS sequences

4. MBS Modeling

4.1 Design procedure

This study considers corner-supported steel braced MBSs with 4, 8, and 12 stories as structural models. The volumetric module is composed of columns, beams, the floor (joists, deck, and concrete topping), and ceiling joists that are rigidly inter-connected. There are 25 modules in total: five in each direction, horizontally and vertically. Module dimensions are 3.6 m wide, 6.1 m long, and 3.1 m high. According to Figure 4(a), each module is modeled with a 200 mm gap between horizontal and vertical axes to account for column offsets and small spaces between columns. Thus, the total heights for 4-, 8-, and 12-story MBS are 13.2 m, 27 m, and 40.6 m, respectively. As shown in Figure 4(b), the plan dimension and other geometrical details are depicted. Units are accessed through the central modules. Structural integrity is ensured through horizontal and vertical interconnections between the modules. A symmetrical distribution of corner X braces provides seismic resistance in combination with perimeter moment resisting frames.

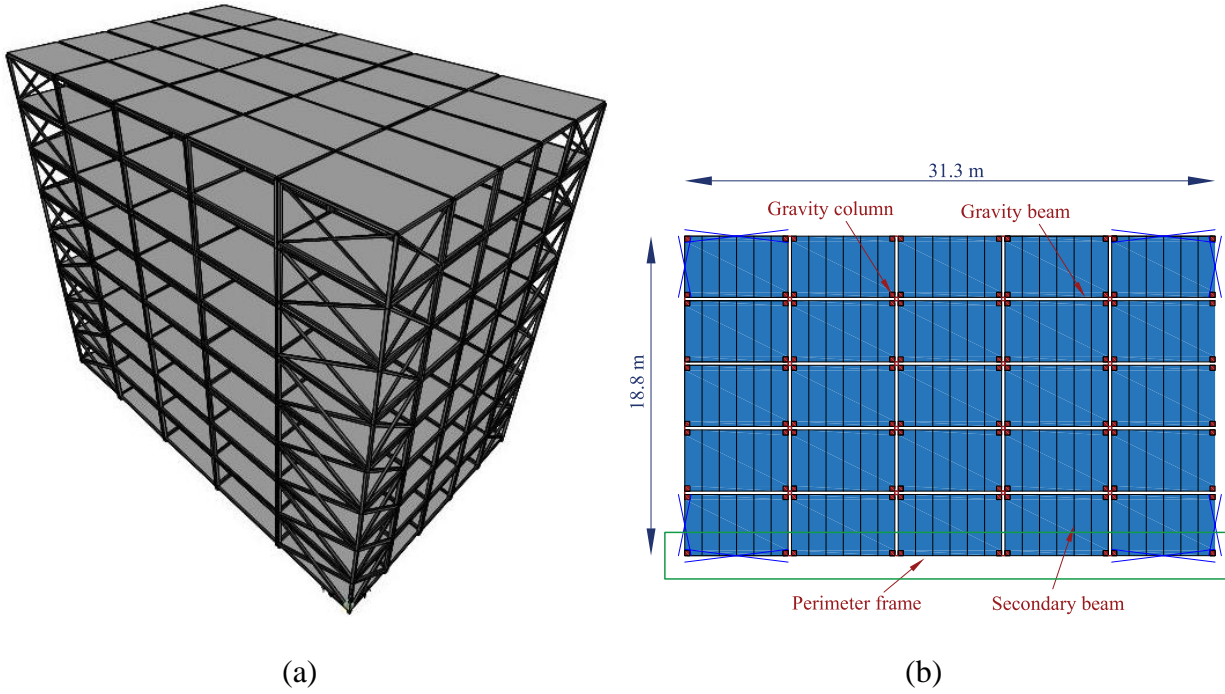


Figure 4 (a) schematic 3D view of the 8-story MBS (b) Plan view of the studied MBSs

SAP2000 software is used to analyze and design the study buildings for risk category II based on ASCE7-16 [51], and AISC [52,53] codes. All studied MBSs were seismically analyzed using the equivalent lateral force (ELF) procedure presented in ASCE7-16. In accordance with this, the MBSs are assumed to be constructed on the site class D. As per FEMA P-695 [54], MBSs are designed with $1.0g S_{DS}$ (short-period spectral acceleration) and $0.6g S_{D1}$ (one-second spectral acceleration). Due to the relatively new nature of these types of structures, there is insufficient research regarding their seismic performance. As a result, the seismic performance factors for “Dual systems with intermediate moment frames” in accordance with ASCE 7-16 are used for the preliminary design of the buildings [55]. Further, a separate diaphragm (one for each module) was considered at each level of the MBS to obtain a more accurate representation of the lateral stiffness of the steel-braced frame and better predictions of the drifts and periods of the building. Table 3 shows the section sizes of columns, beams, and braces. Square hollow sections (HSS) are used for all elements. Similar mechanical properties were given to each selected section, such as 200 GPa modulus of elasticity, 350 MPa yield strength, and 0.3 Poisson's ratio. Connecting adjacent modules is accomplished by using linear link elements. Also, both inter-connections and intra-connections are assigned rigid behavior. Besides the material weight, superimposed dead loads

(SDL) of 0.5 kPa are considered in the design and evaluation of buildings. Live loads on the floor, ceiling, and corridor are 1.92, 0.96, and 4 kPa, respectively.

Table 3 Section sizes for archetypes (units in inch)

Members	4-story	8-story		12-story		
	Story 1-4	Story 1-4	Story 4-8	Story 1-4	Story 4-8	Story 8-12
Column	5×5×1_2	8×8×3_8	6×6×5_16	9×9×5_8	9×9×5_8	7×7×1_2
Floor beam	4×4×3_8	5×5×1_4	5×5×1_4	5×5×5_16	5×5×5_16	5×5×5_16
Ceiling beam	4×4×5_16	4×4×1_4	4×4×1_4	4×4×1_4	4×4×1_4	4×4×1_4
Brace	5×5×1_4	7×7×1_4	5×5×1_4	6×6×1_2	6×6×1_2	5×5×1_2

4.2 Horizontal and Vertical Inter-Module Connection Properties

Both horizontal and vertical inter-module connections (IMCs) are critical for ensuring stability and structural integrity in multi-story corner-supported modular buildings. Especially regarding stiffness and load transfer, The performance of the structure can be significantly affected by these connections. To link modules at their corners, vertical and horizontal inter-module connections (VCs and HCs) were simulated following Styles et al. [56]. A detailed finite element (FE) model was developed in that study for analyzing typical connections of modular structures, emphasizing on the horizontal and vertical ties. By using separate ties and end plates, this system provided vertical and horizontal connectivity independently of one another. Based on the finding by Styles et al., the numerical results include force displacement behavior of horizontal IMCs in the X and Z directions and moment-rotation in the X and Y directions. In contrast, there is no information available regarding the moment rotation of vertical IMCs. The moment-rotation behavior of horizontal connections has been assumed to apply to both vertical and horizontal connections due to insufficient data and in an attempt to simplify the problem [57,58]. Table 4 demonstrates the stiffness properties of the horizontal and vertical of the utilized connection in this study in the axial (Y), shear (Z), and rotational (R). Vertical connections (VCs) are constructed from end plates welded to both ends of the columns, with connectivity achieved by multiple bolts. A similar configuration is applied to horizontal IMCs, which involves welding end-plates to the side faces of columns and bolting them together. The shear and rotational behaviors of bolted endplate IMCs have been experimentally analyzed in references [59,60]. Figure 5 presents a schematic representation of these horizontal and vertical inter-connections.

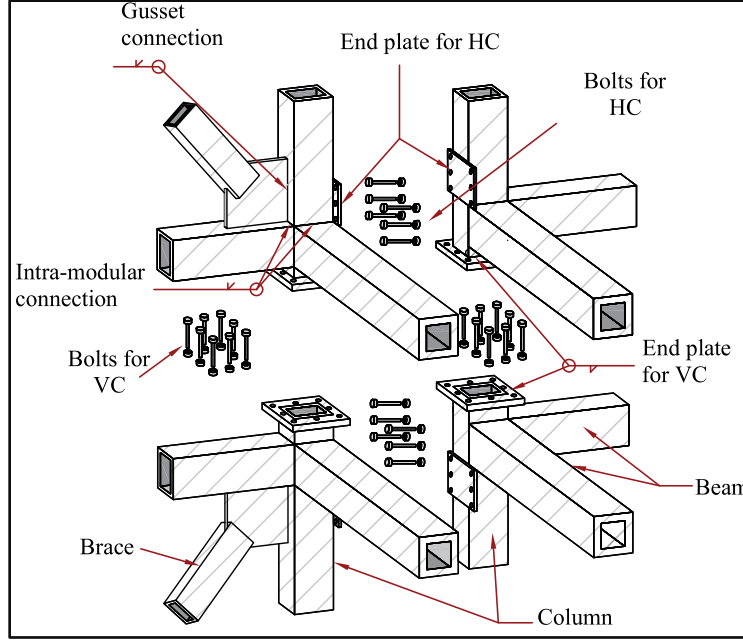


Figure 5 Vertical and horizontal IMC details [56].

Table 4 Stiffness properties of inter-connection

Connection type	HC			VC		
	Y (KN/m)	Z (KN/m)	R (KN.m/rad)	Y (KN/m)	Z (KN/m)	R (KN.m/rad)
Stiffness value	388625	680844	26456.81	1620745	323416	26456.81

4.3 Numerical Modeling

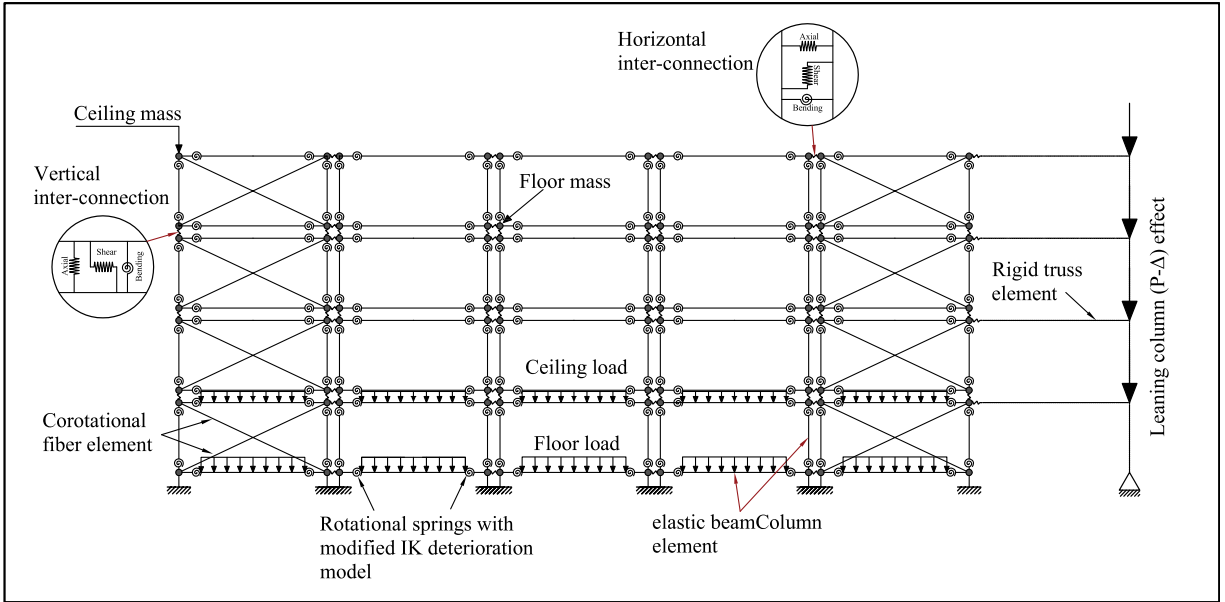
OpenSees software is used as a nonlinear dynamic analysis program. A two-dimensional model along with the leaning columns has been used to model the lateral force-resisting frame located at the perimeter of the building due to its regularity in the plan and elevation. Thus, the perimeter frame illustrated in Figure 4(b) is analyzed, as shown in Figure 6.

Steel grade S350 is used in this research which has a yield strength and ultimate strength of 350 MPa and 450 MPa, respectively. The modulus of elasticity of this material is taken as 200 GPa. This material's stress-strain relationship was defined with the uniaxial material model Steel02 in OpenSees. To represent nonlinear structural behavior, a plastic hinge rotational spring (zero-length element) is used to connect the elastic beam and column elements. These hinges have a moment rotation relationship which is represented by the Ibarra-Median-Krawinkler (IMK) model

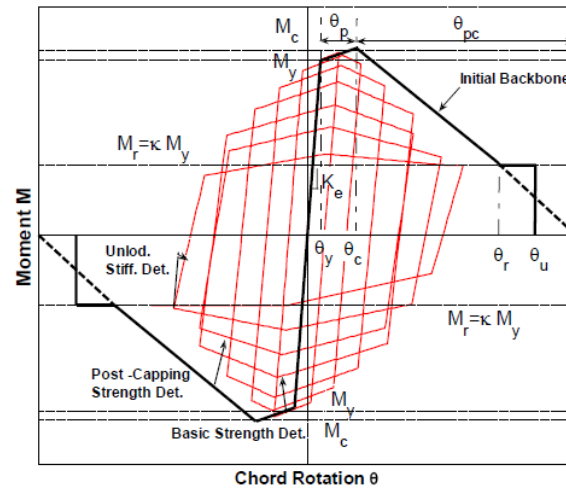
[61] as well as the regression equations provided in [62]. Moments and rotations are mainly described by their yield points $[y, M_y]$ and capping points $[c, M_c]$. The rotation between the yield and capping points is denoted as θ_p , while θ_{pc} is the post-capping plastic rotation. According to [62,63] the parameters necessary for the present study were calculated.

In the two-dimensional model, gravity columns are represented by pin-ended rigid columns rigidly connected to the frame. In each story, the axial load acting on each internal gravity column is equal to the sum of the gravity loads on the leaning column. To account for P-delta effects, elastic beam-column elements with larger cross sections and moments of inertia were employed. A zero-length rotational spring element with a low stiffness was used to connect leaning columns to beam-column joints. Leaning columns and the main frame are related to rigid links by means of truss elements, thereby transferring the effects of P-delta. To consider the second-order effects in OpenSees, the corotational transformation is applied.

In this study, braces are modeled using the method presented by Gunnarsson in previous studies [64]. Herein, the brace's buckling behavior is modeled by using a 10 dispBeamColumn fiber element along its length. An initial displaced shape is considered to predict brace buckling. A sinusoidal function with an amplitude equal to 1/1,000 of the length of the brace is considered in order to predict brace buckling. A brace aligned with single and multiple springs and located at the end of the plate was examined to adequately capture the rotational behavior of out-of-plane gusset plates at the connections. For an accurate assessment of the buckling capacity of a brace, a correct estimate of the stiffness of the gusset plate is essential [65]. To simulate the degradation of strength and stiffness of welded connections, zero-length nonlinear spring elements were used in OpenSees. A detailed description of the brace and gusset plate can be found in Figure 7.



(a)



(b)

Figure 6 (a)Finite Element Details of the considered frame (b) Deterioration Model

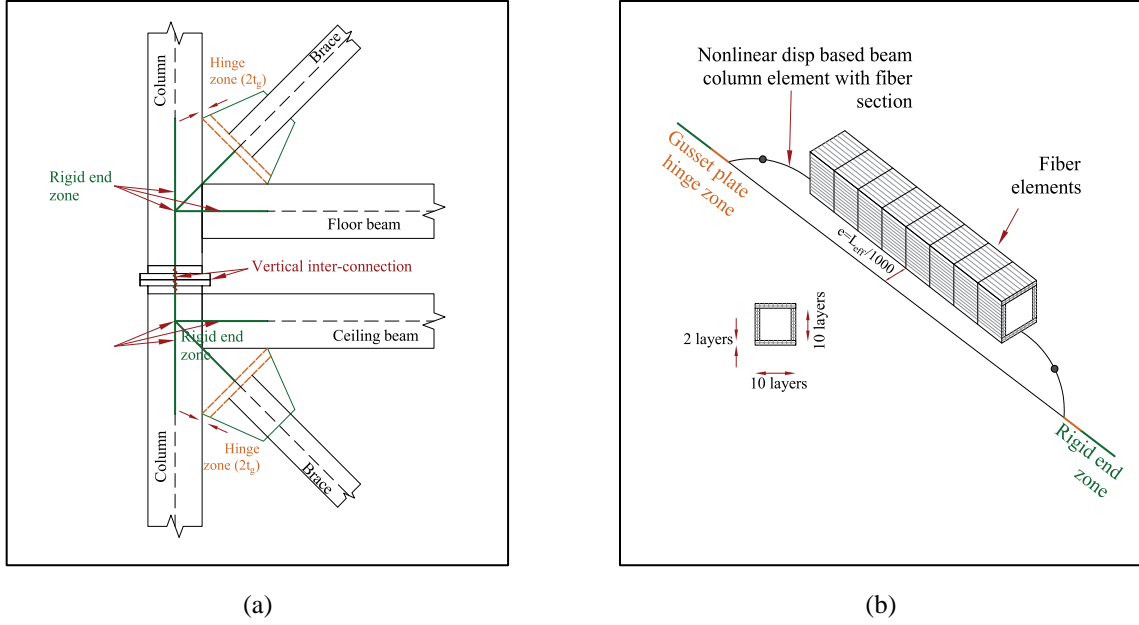


Figure 7 Modeling details of (a) gusset plate (b) buckling behavior of brace [55].

5. Results and Discussion

5.1 Mainshock Analysis

Figure 8 displays the results of IDA for MBSs. According to the spectral acceleration (S_a) trends, the maximum achievable S_a decreases with increasing building height, most likely due to their greater flexibility and an increase in the structural period. Also, the taller buildings reach nonlinearity in lower S_a levels. The four-story building has a greater slope, which means it is much stiffer and more resistant to seismic loads at the beginning. The gentler slopes of the 8-story and 12-story buildings show greater flexibility and a greater tendency for large displacements during seismic events.

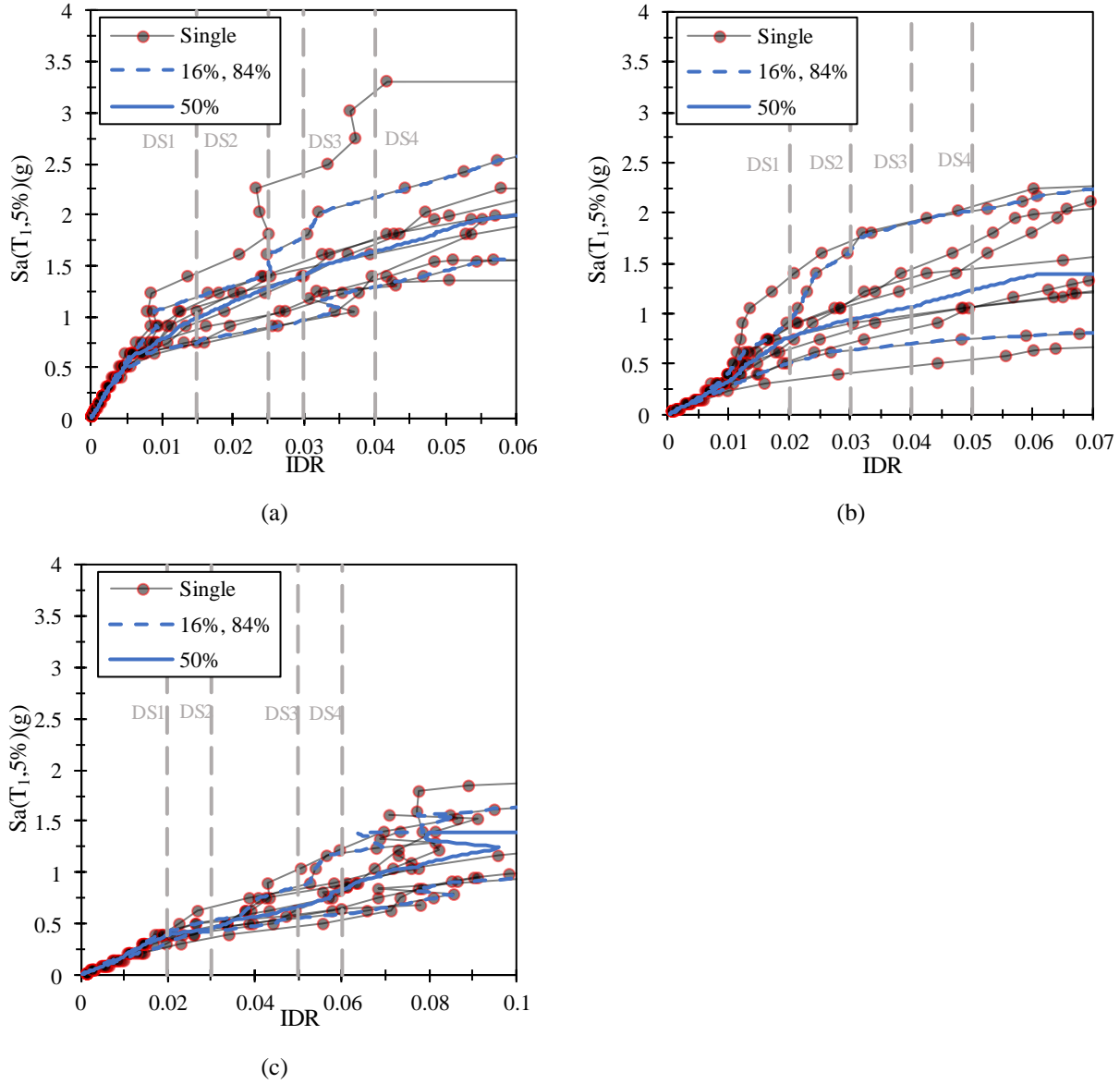


Figure 8 IDA results of MBSs under the mainshock records considering IDR, (a) 4-story (b) 8-story (c) 12-story

Figure 9 shows the IDA results for the 4-story, 8-story, and 12-story modular buildings by plotting spectral acceleration versus the Residual Inter-Story Drift Ratio (RIDR). It is evident from this figure that for the 4-story MBS, the initial slope of the IDA curve is steep; this reflects limited residual deformations. Despite this, the 4-story building shows large residual drifts as the spectral accelerations increase. The relationship between S_a and RIDR in the 8-story building is more moderate than that in the 4-story building, with the RIDR increasing less steeply as S_a increases. Among all the buildings, however, 12-story buildings show the least steep increase in RIDR, indicating their lower sensitivity to changes in spectral acceleration. Considering the number of

stories on a building, with an increase in the number of stories on a building, the failure of MBS increases at low seismic intensities.

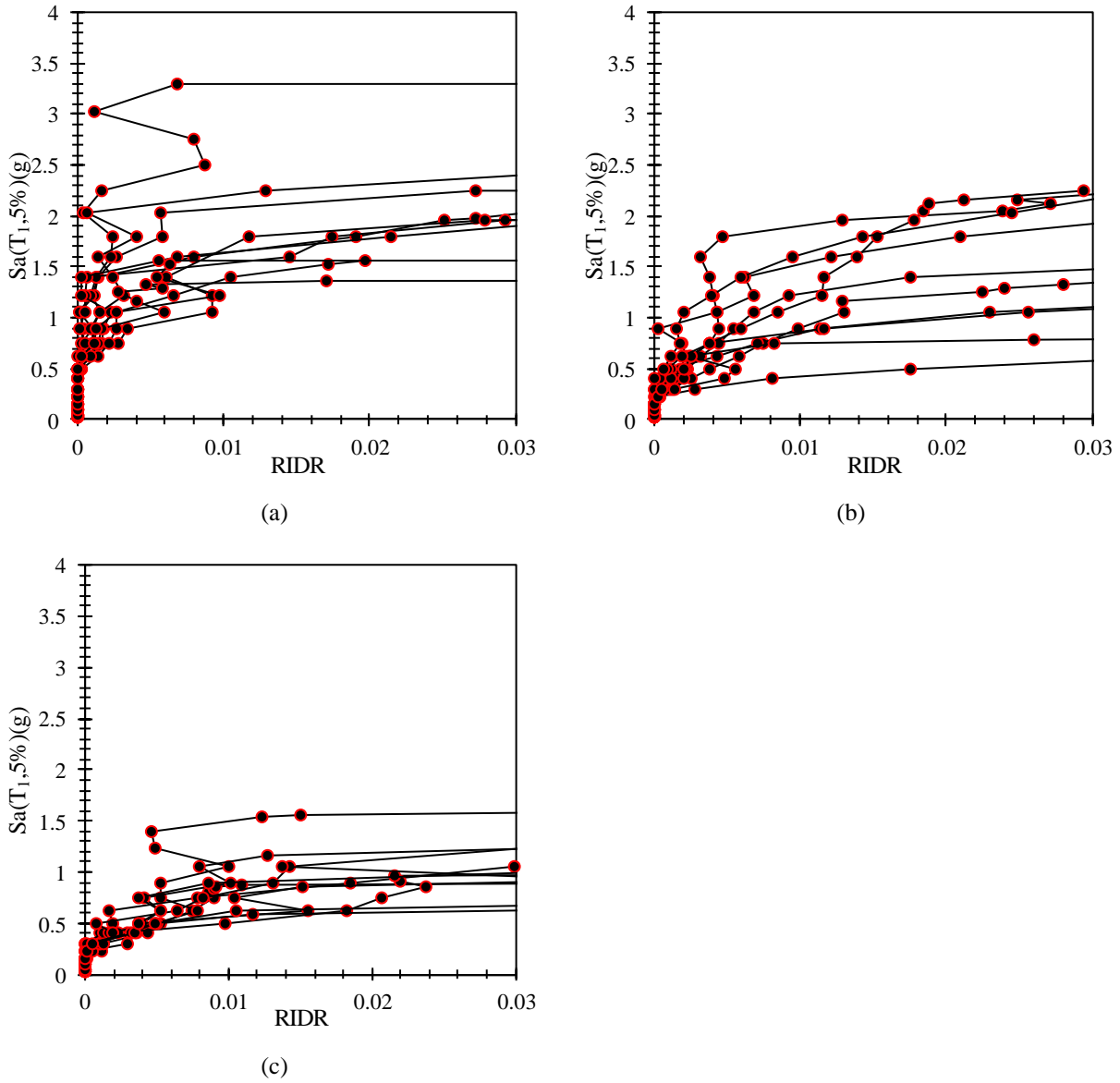


Figure 9 IDA results of MBSs under the mainshock records considering RIDR, (a) 4-story (b) 8-story (c) 12-story

A boxplot of the spectral accelerations of each ground motion associated with each of the four damage states for MBSs is shown in Figure 10. Spectral acceleration normalization was performed to enable meaningful comparisons despite differences in structural periods. The results reveal that as expected, normalized spectral accelerations increase for all building heights when mainshock damage is more severe. The normalized median for DS4 significantly increases from the 4-story to the 8-story building (64% increase), highlighting a notable rise in relative spectral acceleration.

However, the increase from the 8-story to the 12-story building changes minimally. It indicates that taller structures, beyond a certain height, may exhibit similar normalized spectral acceleration behavior under this damage state[66].

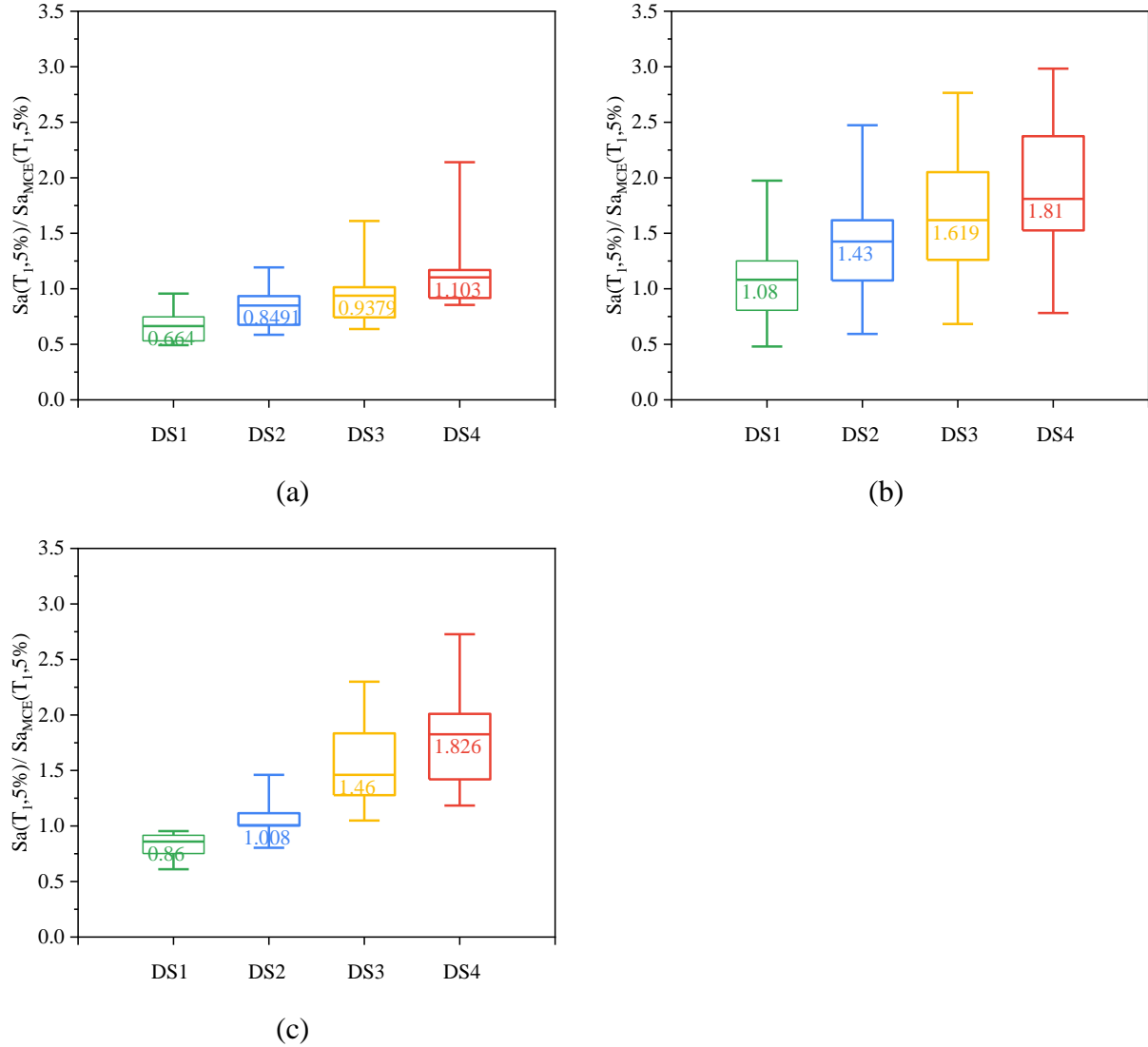


Figure 10 Boxplots of spectral acceleration for (a) 4-story (b) 8-story (c) 12-story modular steel buildings

5.2 Mainshock-Aftershock Analysis

The roof drift time-history response of an 8-story modular steel building subjected to a mainshock (GM2) followed by aftershocks (GM4) at increasing intensities (0.4g, 0.85g, and 1.0g) is depicted in Figure 11. The initial mainshock induces DS2 (IDR=0.03) and causes 0.48% of residual roof drift (RRD). The subsequent residual roof drifts induced in the various aftershocks are accordingly

0.47%, 1.40%, and 2.0% each, demonstrating an accumulation of permanent deformation. This highlights the progressive damage caused by aftershocks, which signals the need to consider aftershock sequences when assessing the seismic resilience of modular steel structures and thus the contribution of this research study.

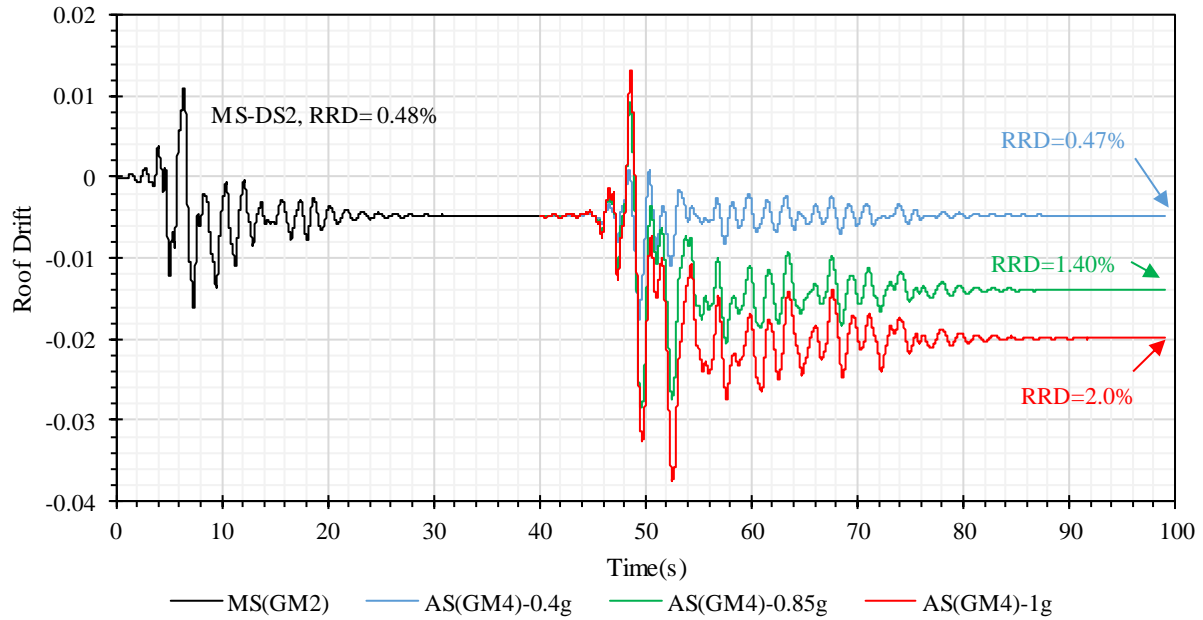


Figure 11 Roof drift results for the 8-story MBS under mainshock-aftershock sequences with the same AS records but different intensities.

Figure 12 illustrates the time history of roof drift in the 12-story MBS after a mainshock (GM1) followed by several aftershocks of constant intensity. A mainshock causes initial damage (DS2) to the structure, placing it in a vulnerable state, while subsequent aftershocks cause further damage. In the figure, the point of structural collapse is evident as one of the aftershock records results in a significant negative value of roof drift that leads to collapse. A collapse of this nature indicates the modular building's reduced capacity to resist additional seismic loads after mainshock damage. Even though the intensities are equal for the aftershocks, the underlying variability in the aftershock responses really points to the consideration of seismic design for aftershock sequences, as the accumulation of damage can dramatically reduce structural resilience, result in the potential failure of the structures under repeated earthquakes.

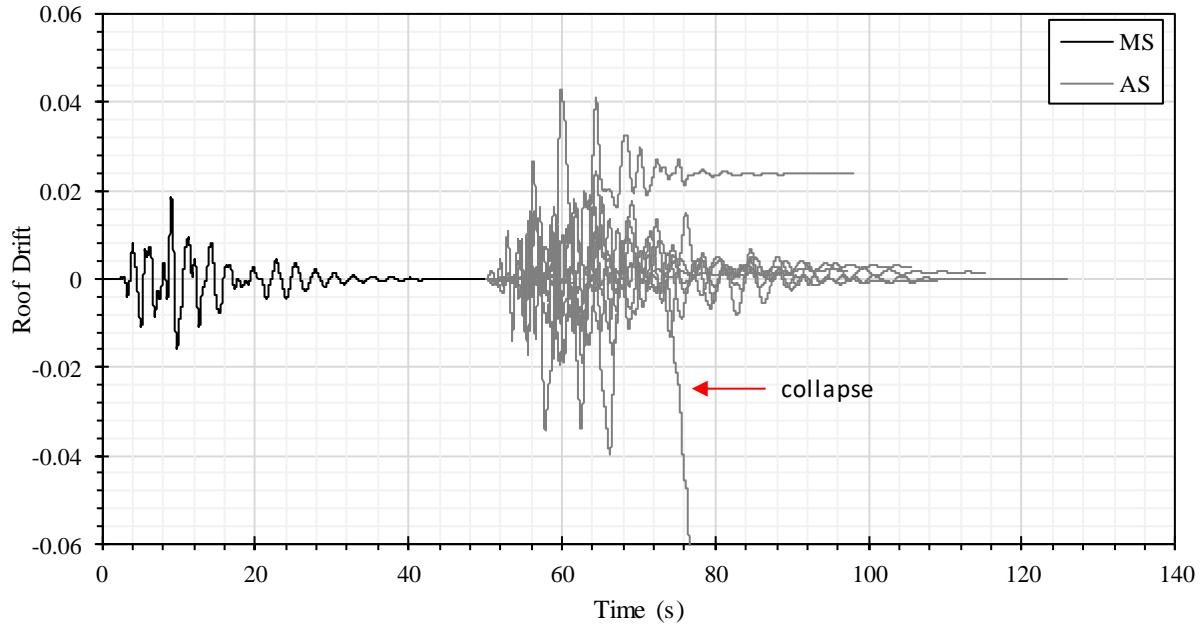


Figure 12 Roof drift results for the 8-story MBS under mainshock-aftershock sequences with the different AS records at $S_a(T_1, 5\%) = 0.75g$.

Figure 13 analyzes the relationship between the RIDR and various damage states (DS) for modular buildings with 4, 8, and 12 stories, using FEMA P-58 criteria. A comparison of median RIDR values observed across these building types was conducted with estimates based on FEMA's IDR thresholds.

The findings indicate that while the median RIDR values for DS1 align well with FEMA's predictions, indicating reasonable accuracy for minor damage, the median RIDR values for DS2 through DS4 consistently fall below the expectations of FEMA. In particular, the 8-story and 12-story modular buildings, particularly at DS3 and DS4, illustrate a tendency to overestimate RIDR by FEMA guidelines as the severity of damage increases. This may indicate that FEMA P-58 overestimates the residual drifts in modular buildings. These differences can be explained by unique structural features of modular constructions, such as inter-module connections and discrete diaphragms. Therefore, developing an assessment methodology specifically for modular construction will be desirable.

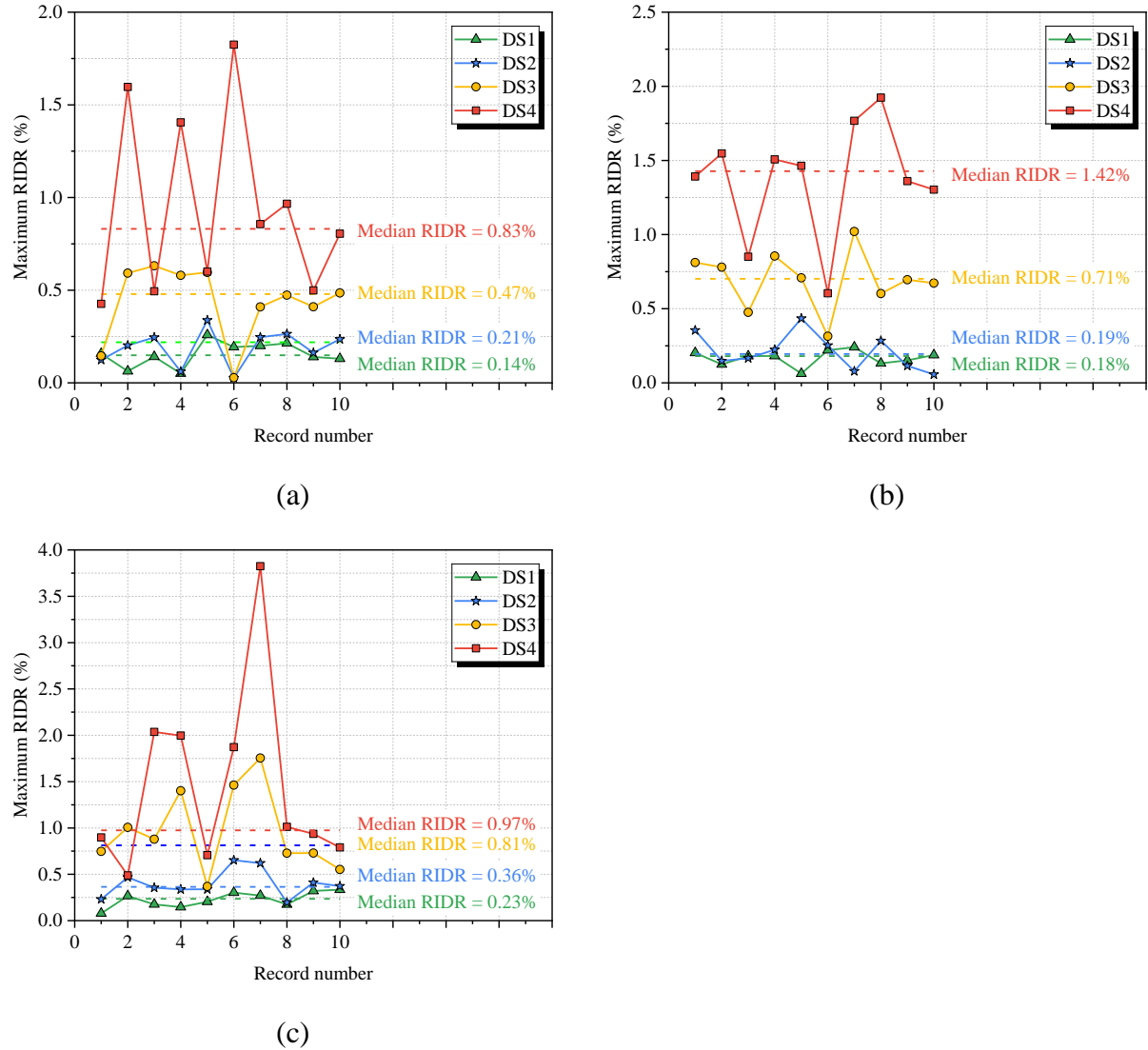


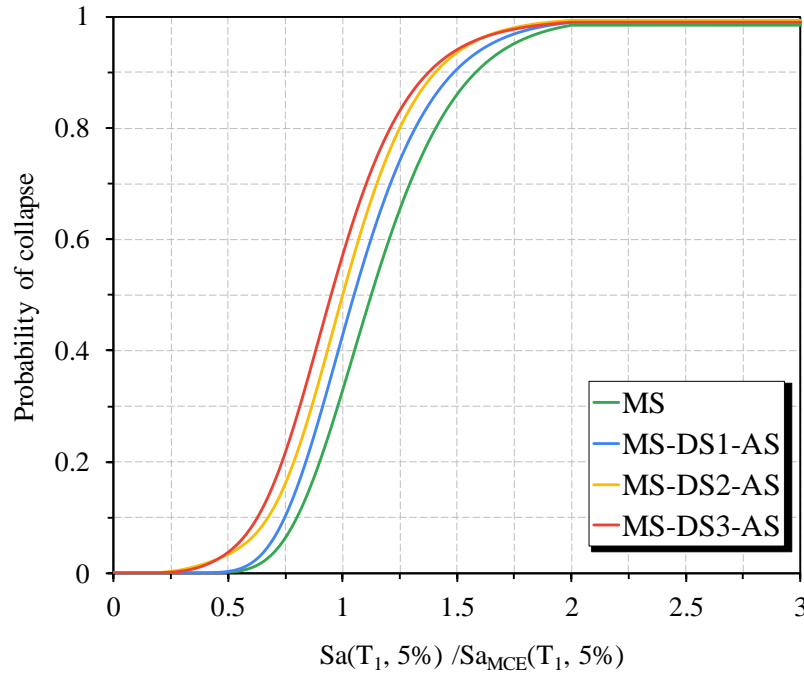
Figure 13 The maximum residual inter-story drift ratio of (a) 4-story (b) 8-story (c) 12-story modular steel buildings subjected to mainshocks scaled at four IDR-based damage states

The fragility curves for all buildings under mainshock-only (MS) and mainshock-aftershock (MS-AS) scenarios in Figure 14 illustrate how the likelihood of collapse varies with seismic intensity. Buildings that experienced more severe damage from the MS were found to be significantly more vulnerable to collapse during subsequent aftershocks. Across all building heights, aftershocks that follow a mainshock are associated with an increased likelihood of collapse with the effect increasing as the damage state increases from DS1 to DS3. The results suggest that shorter buildings are generally more susceptible to collapse, with the 4-story building showing a notably higher risk of collapse under these conditions. While the "mainshock only" scenario consistently exhibits greater resilience across all heights, the MS-DS3-AS scenario highlights a significant

vulnerability, especially in the 8-story building, where the gap in performance between different damage states becomes particularly pronounced.

The 4-story building shows a pronounced increase in fragility between damage states, suggesting that shorter modular buildings are more vulnerable to cumulative damage and aftershocks. In contrast, the 8-story and 12-story modular buildings show a more gradual change in fragility, indicating that taller and more flexible structures are better able to manage cumulative damage, even though they become more susceptible as the damage continues to accumulate. As compared to lower structures, the 12-story modular building has more closely spaced curves; this could be due to the fact that more redundancy in high-rise structures supplies more paths for transferring the load after the failure of a member[67].

Overall, these findings emphasize the crucial impact of modular building height and pre-existing damage on the vulnerability of modular structures to seismic forces. This highlights the importance of customized design strategies for earthquake-prone regions to enhance resilience and reduce the risk of collapse.



(a)

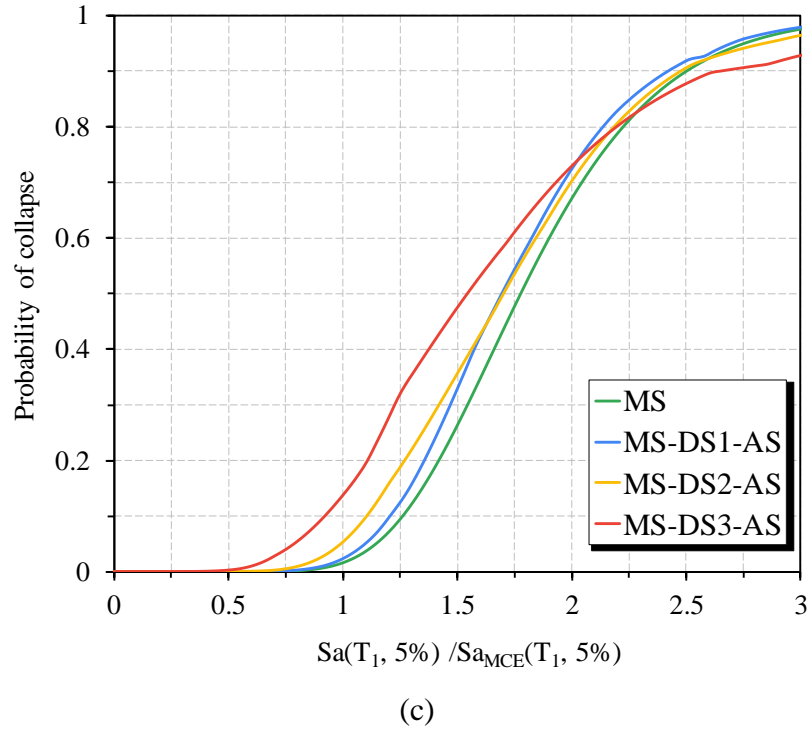
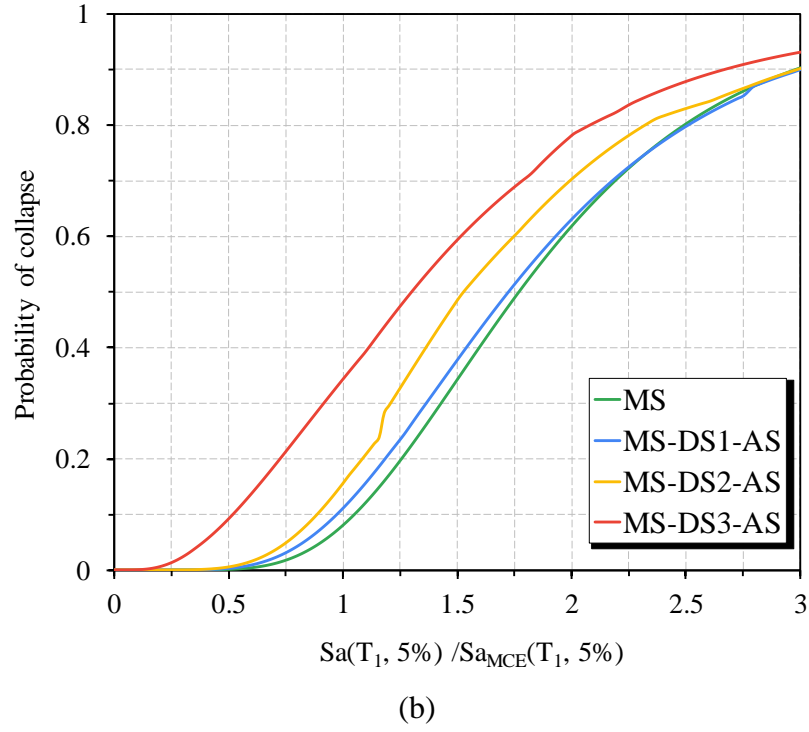


Figure 14 the results of fragility curves for different MS-AS scenarios: (a) 4-story (b) 8-story (c) 12-story

5.3 Collapse Margin Ratio (CMR)

In performance-based seismic design, the Collapse Margin Ratio (CMR) is a critical metric, reflecting the resilience of a structure under seismic loading. It is a useful index to evaluate global seismic anti-collapse resistance of structures and is defined as the ratio of a building's median collapse capacity to the spectral acceleration at the design level, typically associated with the Maximum Considered Earthquake (MCE). A Collapse Margin Ratio (CMR) greater than 1.0 shows that a structure can endure ground motions beyond its design capacity, offering a safety margin against collapse. On the other hand, a CMR below 1.0 indicates a heightened risk of collapse under expected seismic conditions. This ratio is especially useful in IDAs as it measures the building's performance across different seismic intensities, helping to evaluate the structure's safety and resilience in potential earthquake scenarios. IDA is used to determine the median collapse capacity of structures according to Eq. 9 and the collapse margin ratio of structures according to Eq. 10.

$$S_{CT} = \text{Median} (S_{a, \text{Collapse}}) \quad (9)$$

$$CMR = \frac{S_{CT}}{S_{MT}} \quad (10)$$

Where S_{CT} represents the median collapse capacity obtained from IDA for all records, $S_{a, \text{Collapse}}$ represents the collapse capacity obtained from IDA for each record, and S_{MT} represents the spectral acceleration that corresponds to the maximum Considered Earthquake in the fundamental period of the structure.

MCE earthquakes have a probability of occurring every 50 years of 2%, according to ASCE. MCE's acceleration response spectrum is 1.5 times that of a DBE's. As mentioned earlier, the S_{DC} of D_{max} was considered in this study. In accordance with ASCE 7-10, the approximate fundamental period of the structure is:

$$T_a = C_t \times h_n^x \quad (11)$$

where, h_n is structure height, and c_t and x are coefficients calculated from table 12.8-2, depending on structure type, with values of 0.0488 and 0.75 given. The following equation determines the fundamental period of the structure, T :

$$T = C_u \times T_a \quad (12)$$

where C_u is taken 1.5 as S_{D1} is greater than 0.4. The transition period (T_s) can be calculated as:

$$T_s = \frac{S_{D1}}{S_{DS}} \quad (13)$$

Based on the comparison of the T and T_s , the design spectral acceleration of the structure can be determined:

$$S_a = S_{DS} \text{ For } T < T_s \quad (14)$$

$$S_a = \frac{S_{D1}}{T} \text{ For } T_s < T < T_L \text{ (long period)} \quad (15)$$

Table 5 shows calculated values for 4-, 8-, and 12-story buildings. The corresponding median S_{CT} under mainshock records for these structures is 1.65, 1.25, and 0.83, respectively.

Table 5 Spectral acceleration values for MBSs at the MCE level

Archetypes	$T_{1, \text{software}}(\text{s})$	height (m)	$T_a(\text{s})$	$T(\text{s})$	$S_a(T_1, 5\%)$	$S_{aMT}(T_1, 5\%)$
4-story	0.51	13.2	0.34	0.47	1	1.5
8-story	1.3	27	0.58	0.81	0.74	1.11
12-story	1.99	40.6	0.78	1.1	0.55	0.82

Fig. 15 shows the median CMR in the 4-, 8-, and 12-story modular buildings under MS-only and MS-AS sequences at different damage states. For all buildings, CMR is greater than one under the mainshock-only scenario, which reflects resiliency more than design expectations. For MS-AS sequences, however, the CMR is less than 1 for all building heights and damage states, except for the 12-story building in MS-DS1-AS and MS-DS2-AS scenarios. This reduced CMR indicates that aftershocks increase the probability of collapse after a primary mainshock. The maximum reduction in CMR corresponds to the MS-DS3-AS scenario, implying that pre-damaged buildings are more susceptible to aftershock effects. These results underscore the importance of accounting for aftershocks within modular building design to improve post-mainshock resilience and to minimize the risk of collapse.

In addition, it is important to note that under the mainshock-only records, CMR for the designed steel modular buildings may approach the collapse threshold under maximum considered

earthquake (MCE) conditions due to the proximity to 1.0 for these structures. Although further research is required for its validation, these relatively low CMR values hint that the seismic design parameters used may not fully align with the specific behavior and performance needs of modular buildings specifically the seismic modification factor used, and the spectral acceleration values of $SDS = 1.0$ and $SD1 = 0.6$ recommended by FEMA P-695 for seismic design category D_{max} . The greater value of CMR would improve the seismic collapse resistance of modular structures in earthquake-prone areas by providing an added safety margin against collapse.

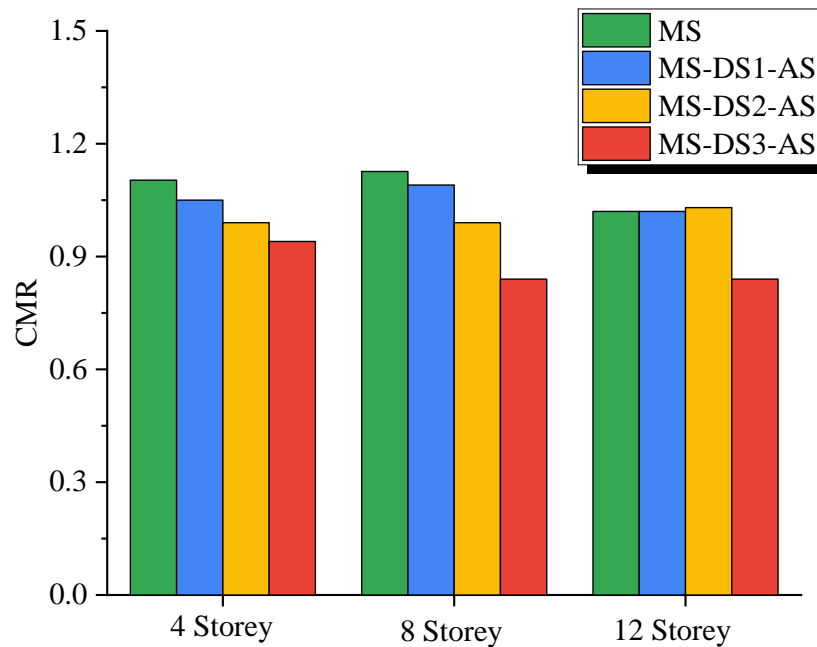


Figure 15 The values of collapse margin ratio for only MS and MS-AS scenarios

The following Table 6 summarizes CMR values for all the modular buildings under varied seismic scenarios. CMR value for the mainshock-only ranged from 1.02 to 1.126 across the different building heights. However, as aftershock scenarios progressed from MS-DS1-AS to MS-DS3-AS, a notable decline in CMR was observed, particularly in the 8-story building, which experienced a 25.03% reduction at the most severe damage state (DS3). In the case of the 4-story building, there is a gentler drop in the CMR, while for the 12-story building, resistance was up to the initial damage states and then suddenly dropped 16.11% at DS3. These results suggest that taller buildings might be more vulnerable to severe damage when aftershocks occur and point to the importance of considering building height in seismic design and assessment.

Table 6 Values of CMR along with the differences of MS-AS sequences with only MS scenario

Seismic scenarios	4st	Difference with MS(%)	8st	Difference with MS(%)	12st	Difference with MS(%)
MS	1.103	---	1.126	---	1.020	---
MS-DS1-AS	1.05	4.85	1.09	2.88	1.02	1.50
MS-DS2-AS	0.99	10.30	0.99	11.60	1.03	1.86
MS-DS3-AS	0.94	14.52	0.84	25.03	0.84	16.11

6. Concluding Remarks

The purpose of this study was to investigate the seismic performance of steel volumetric modular building systems (MBSs) under a sequence of mainshock-aftershock (MS-AS) records for the first time. OpenSees software was used to model three typical MBSs. Incremental dynamic analyses (IDA) of mainshocks were conducted to determine the spectral acceleration demands corresponding to specific damage states. Four mainshock damage states have been defined based on FEMA P-58 to induce these damage levels on the selected modular buildings. IDAs of aftershocks were then conducted to assess the performance of each MBS under MS-AS conditions.

According to the comparison of the residual inter-story drift ratio obtained from IDAs and FEMA P-58, estimates of the latter are generally conservative, especially for higher damage states (DS2 to DS4). As the severity of damage increases, the 8- and 12-story buildings, particularly at DS3 and DS4, showed a tendency to overestimate the peak residual inter-story drift (RIDR) as prescribed by FEMA guidelines. According to the fragility curves, aftershocks following a mainshock increased the likelihood of collapse across all building heights with this effect increasing as the damage state increased from DS1 to DS3. This highlights the importance of considering the cumulative effects of multiple seismic events rather than just a single event. Furthermore, taller MBSs have a greater ability to withstand cumulative damage than shorter ones. It is evident from these results that aftershock considerations must be incorporated into the design and assessment of modular buildings. The calculated Collapse Margin Ratios (CMRs) further highlight this vulnerability, as modular structures demonstrate relative resilience in single mainshock scenarios but experience notable declines in CMR values following MS-AS sequences. In particular for the 12-story building, the CMR in high-damage aftershock scenarios drops below the collapse threshold. The results show that modifying the design parameters considering the unique behavior that modular buildings depict under sequential seismic loading will improve

resilience and safety. This research therefore advocates for the development of specific seismic assessment frameworks for modular steel buildings that would enhance resilience through performance-based design adaptations in earthquake-prone regions by considering both mainshock and aftershock events. Other subtypes of MBSs could also be explored thereafter in order to generalize these observations.

References

- [1] Hosseinpour F, Abdelnaby AE. Fragility curves for RC frames under multiple earthquakes. *Soil Dyn Earthq Eng* 2017;98:222–34.
- [2] Zhou Z, Han M, Dong Y, Yu X. Seismic resilience of corroded mid-rise reinforced concrete structures under mainshock-aftershock sequences. *Eng Struct* 2023;288:116192.
- [3] Mohammadgholipour A, Billah AHMM. Performance-based plastic design and seismic fragility assessment for chevron braced steel frames considering aftershock effects. *Soil Dyn Earthq Eng* 2024;178:108440.
- [4] Du M, Zhang S, Wang C, She L, Li J, Lu T. Seismic fragility assessment of aqueduct bent structures subjected to mainshock-aftershock sequences. *Eng Struct* 2023;292:116505.
- [5] Alembagheri M, Sharafi P, Rashidi M, Bigdeli A, Farajian M. Natural dynamic characteristics of volumetric steel modules with gypsum sheathed LSF walls: Experimental study. *Structures*, vol. 33, 2021, p. 272–82.
- [6] Sharafi P, Rashidi M, Alembagheri M, Bigdeli A. System Identification of a Volumetric Steel Modular Frame Using Experimental and Numerical Vibration Analysis. *J Archit Eng* 2021;27:04021032. [https://doi.org/10.1061/\(asce\)ae.1943-5568.0000498](https://doi.org/10.1061/(asce)ae.1943-5568.0000498).
- [7] Farajian M, Sharafi P, Bigdeli A, Eslamnia H, Rahnamayiezekavat P. Experimental Study on the Natural Dynamic Characteristics of Steel-Framed Modular Structures. *Buildings* 2022;12:587.
- [8] Rashidi M, Sharafi P, Alembagheri M, Bigdeli A, Samali B. Operational modal analysis, testing and modelling of prefabricated steel modules with different lsf composite walls. *Materials (Basel)* 2020;13:1–18. <https://doi.org/10.3390/ma13245816>.

- [9] Bigdeli A, Emamikoupaei A, Tsavdaridis KD. Probabilistic seismic demand model and optimal intensity measures for mid-rise steel modular building systems (MBS) under near-field ground motions. *J Build Eng* 2023;105916.
- [10] Sharafi P, Rashidi M, Alembagheri M, Bigdeli A. System identification of a volumetric steel modular frame using experimental and numerical vibration analysis. *J Archit Eng* 2021;27:4021032.
- [11] Thai H-T, Ngo T, Uy B. A review on modular construction for high-rise buildings. *Structures*, vol. 28, 2020, p. 1265–90.
- [12] Lawson RM, Ogden RG, Bergin R. Application of modular construction in high-rise buildings. *J Archit Eng* 2012;18:148–54.
- [13] Srisangeerthan S, Hashemi MJ, Rajeev P, Gad E, Fernando S. Review of performance requirements for inter-module connections in multi-story modular buildings. *J Build Eng* 2020;28:101087.
- [14] Liu J, Chen Z, Liu Y, Bai Y, Zhong X. Full-scale corner-supported modular steel structures with vertical inter-module connections under cyclic loading. *J Build Eng* 2021;44:103269.
- [15] Pang R, Yang Y, Zhou Y, Jing M, Xu B. Seismic reliability analysis of high earth-rockfill dams subjected to mainshock-aftershock sequences using a novel noninvasive stochastic finite element method. *Soil Dyn Earthq Eng* 2024;183:108817.
- [16] Aghaeipoor M, Alembagheri M. Seismic damage of submerged intake tower under the sequence of mainshocks and aftershocks. *J Earthq Eng* 2022;26:6893–917.
- [17] Ashna KN, Maheshwari P, Viladkar MN. Fragility analysis of a concrete gravity dam under mainshock-aftershock sequences. *Structures*, vol. 61, 2024, p. 106117.
- [18] Liu J, Tian L, Meng X, Yang M. Seismic fragility assessment of a transmission tower considering mainshock-aftershock sequences. *J Constr Steel Res* 2022;194:107344.
- [19] Liu J, Tian L, Yang M, Meng X. Probabilistic framework for seismic resilience assessment of transmission tower-line systems subjected to mainshock-aftershock sequences. *Reliab Eng Syst Saf* 2024;242:109755.
- [20] Jing W, Zhang Y, Wang Q, Song S. Dynamic responses of non-isolated and isolated liquid

- storage tanks under mainshock-aftershock sequences. *Structures*, vol. 69, 2024, p. 107347.
- [21] Chen X, Xiang N, Guan Z, Li J. Seismic vulnerability assessment of tall pier bridges under mainshock-aftershock-like earthquake sequences using vector-valued intensity measure. *Eng Struct* 2022;253:113732.
- [22] Cui Z-D, Sui T-Y, Wang S-Y, Yuan L. Seismic response of subway station subjected to mainshock-aftershock sequences by centrifuge shaking table tests. *Soil Dyn Earthq Eng* 2024;176:108327.
- [23] Wang J, Wang H, Pan P, Wang G, Xu Z, Zhao D, et al. Endurance time analysis for seismic performance of underground structures subjected to mainshock--aftershock sequences. *Eng Struct* 2024;306:117879.
- [24] Zhang Y, Wang Z, Jiang L, Skalomenos K, Zhang D. Seismic fragility analysis of masonry structures considering the effect of mainshock-aftershock sequences. *Eng Struct* 2023;275:115287.
- [25] Zhang Y, Wang Z, Jiang L, Skalomenos K, Zhang D. Seismic analysis method of unreinforced masonry structures subjected to mainshock-aftershock sequences. *Bull Earthq Eng* 2022;20:2619–41.
- [26] Koochfallah K, Dehkordi MR, D'Ayala D, Amiri GG, Eghbali M, Samadian D. Seismic resilience of typical steel school building and retrofitting options based on FEMA P-58 under mainshock-aftershock effects. *J Build Eng* 2024;86:108636.
- [27] Rayegani A, Soureshjani OK, Alaei SAM, Mualla IH, Nemati F. Seismic Performance of Buildings Equipped with Four-Joint Rotational Friction Dampers in Mainshock--Aftershock Sequences. *J Struct Eng* 2024;150:4023235.
- [28] Saed G, Balomenos GP. Fragility framework for corroded steel moment-resisting frame buildings subjected to mainshock-aftershock sequences. *Soil Dyn Earthq Eng* 2023;171:107975.
- [29] Fang C, Ping B, Zheng Y, Ping Y, Ling H. Seismic fragility and loss estimation of self-centering steel braced frames under mainshock-aftershock sequences. *J Build Eng* 2023;73:106433.

- [30] Jalali SA, Amini A, Mansouri I, Hu JW. Seismic collapse assessment of steel plate shear walls considering the mainshock--aftershock effects. *J Constr Steel Res* 2021;182:106688.
- [31] Torfehnejad M, Sensoy S. Energy absorption and inelasticity distribution mechanisms in steel moment frames affected by mainshock-aftershock sequences. *Structures*, vol. 33, 2021, p. 3550–69.
- [32] Shafaei H, Naderpour H. Collapse capacity of ordinary RC moment frames considering mainshock-aftershock effects. *J Earthq Eng* 2022;26:5318–37.
- [33] Shi F, Saygili G, Ozbulut OE, Zhou Y. Risk-based mainshock-aftershock performance assessment of SMA braced steel frames. *Eng Struct* 2020;212:110506.
- [34] Hassan EM, Admuthe S, Mahmoud H. Response of semi-rigid steel frames to sequential earthquakes. *J Constr Steel Res* 2020;173:106272.
- [35] Emamikoupaei A, Bigdeli A, Tsavdaridis KD. Nonlinear seismic response of mid-rise modular buildings subjected to near-field ground motions. *J Constr Steel Res* 2023;201:107696.
- [36] Fathieh A, Mercan O. Seismic evaluation of modular steel buildings. *Eng Struct* 2016;122:83–92. <https://doi.org/10.1016/j.engstruct.2016.04.054>.
- [37] Batukan MB, Sanches R, Hashemi A, Mercan O, Fathieh A, Quenneville P. Seismic performance of modular steel buildings (MSBs) equipped with resilient slip friction joints (RSFJs). *J Build Eng* 2022;47:103881.
- [38] Annan CD, Youssef MA, El Naggar MH. Seismic vulnerability assessment of modular steel buildings. *J Earthq Eng* 2009;13:1065–88.
- [39] Chua YS, Liew JYR, Pang SD. Modelling of connections and lateral behavior of high-rise modular steel buildings. *J Constr Steel Res* 2020;166:105901.
- [40] Peng J, Hou C, Shen L. Numerical analysis of corner-supported composite modular buildings under wind actions. *J Constr Steel Res* 2021;187:106942. <https://doi.org/10.1016/j.jcsr.2021.106942>.
- [41] Lacey AW, Chen W, Hao H, Bi K. Lateral behaviour of modular steel building with simplified models of new inter-module connections. *Eng Struct* 2021;236:112103.

- [42] Di Sarno L, Elnashai A. Fundamentals of earthquake engineering. John Wiley Sons, Ltd, Available In< [Http//Media Wiley Com/Product_data/Excerpt/36/04700248/0470024836 Pdf](http://Media.Wiley.Com/Product_data/Excerpt/36/04700248/0470024836.Pdf)>, Retrieved June 2008;1:2014.
- [43] Vamvatsikos D, Cornell CA. Incremental dynamic analysis. *Earthq Eng Struct Dyn* 2002;31:491–514.
- [44] FEMA 350. Recommended seismic design criteria for new steel moment-frame buildings. 2000.
- [45] Miano A, Jalayer F, Ebrahimian H, Prota A. Cloud to IDA: Efficient fragility assessment with limited scaling. *Earthq Eng Struct Dyn* 2018;47:1124–47.
- [46] Amiri S, Bojórquez E. Residual displacement ratios of structures under mainshock-aftershock sequences. *Soil Dyn Earthq Eng* 2019;121:179–93.
- [47] Ruiz-Garcia J, Miranda E. Probabilistic estimation of residual drift demands for seismic assessment of multi-story framed buildings. *Eng Struct* 2010;32:11–20.
- [48] Kazantzi AK, Vamvatsikos D. The hysteretic energy as a performance measure in analytical studies. *Earthq Spectra* 2018;34:719–39.
- [49] Ruiz-García J, Aguilar JD. Aftershock seismic assessment taking into account postmainshock residual drifts. *Earthq Eng Struct Dyn* 2015;44:1391–407.
- [50] Fema P. 58-1, Seismic performance assessment of buildings volume 1-methodology. Appl Technol Counc Calif Redw City 2012.
- [51] of Civil Engineers (ASCE) AS. ASCE/SEI 7-16: Minimum Design Loads for Buildings and Other Structures, 2016.
- [52] 360-10 A. Specification for structural steel buildings. Am Inst Steel Constr 2010.
- [53] AISC 341. Seismic provisions for structural steel buildings. Am Inst Steel Constr Chicago, Illinois 2010.
- [54] FEMA P695. Quantification of building seismic performance factors. US Department of Homeland Security, FEMA; 2009.
- [55] Farajian M, Kildashti K, Sharafi P, Eslamnia H. Quantification of seismic performance

- factors for modular corner-supported steel bracing system. *Structures*, vol. 45, 2022, p. 257–74.
- [56] Styles AJ, Luo FJ, Bai Y, Murray-Parkes JB. Effects of joint rotational stiffness on structural responses of multi-story modular buildings. *Transform. Futur. Infrastruct. through Smarter Inf. Proc. Int. Conf. Smart Infrastruct. Constr.* 27--29 June 2016, 2016, p. 457–62.
 - [57] Alembagheri M, Sharafi P, Tao Z, Hajirezaei R, Kildashti K. Robustness of multistory corner-supported modular steel frames against progressive collapse. *Struct Des Tall Spec Build* 2021;30:e1896.
 - [58] Corfar D-A, Tsavdaridis KD. A comprehensive review and classification of inter-module connections for hot-rolled steel modular building systems. *J Build Eng* 2022;50:104006.
 - [59] Liu XC, He XN, Wang HX, Zhang AL. Compression-bend-shearing performance of column-to-column bolted-flange connections in prefabricated multi-high-rise steel structures. *Eng Struct* 2018;160:439–60.
 - [60] Liu XC, He XN, Wang HX, Yang ZW, Pu SH, Ailin Z. Bending-shear performance of column-to-column bolted-flange connections in prefabricated multi-high-rise steel structures. *J Constr Steel Res* 2018;145:28–48.
 - [61] Ibarra LF, Medina RA, Krawinkler H. Hysteretic models that incorporate strength and stiffness deterioration. *Earthq Eng Struct Dyn* 2005;34:1489–511.
 - [62] Lignos DG, Krawinkler H. Deterioration modeling of steel components in support of collapse prediction of steel moment frames under earthquake loading. *J Struct Eng* 2011;137:1291–302.
 - [63] Lignos DG, Krawinkler H, Whittaker AS. Prediction and validation of sidesway collapse of two scale models of a 4-story steel moment frame. *Earthq Eng Struct Dyn* 2011;40:807–25.
 - [64] Gunnarsson IR. Numerical performance evaluation of braced frame systems. University of Washington, 2004.
 - [65] Hsiao P-C. Seismic performance evaluation of concentrically braced frames. University of Washington; 2012.

- [66] Gatti M. Relation between dynamic amplification, structural height and damage in buildings affected by the recent Italian earthquakes. *Geomatics, Nat Hazards Risk* 2020;11:1154–74.
- [67] Emamikoupaei A, Tsavdaridis KD, Bigdeli A, Saffarzadeh K. Fragility-based robustness assessment of steel modular building systems: Connection and building height. *J Constr Steel Res* 2025;226:109199.